

# Bath-free squeezed phonon lasing via intrinsic ion-phonon coupling

Chen-Yu Lee<sup>1</sup> and Guin-Dar Lin<sup>1,2,3</sup>

<sup>1</sup>*Physics Division, National Center for Theoretical Sciences, Taipei 10617, Taiwan*

<sup>2</sup>*Department of Physics and Center for Quantum Science and Engineering, National Taiwan University, Taipei 10617, Taiwan*

<sup>3</sup>*Trapped-Ion Quantum Computing Laboratory, Hon Hai Research Institute, Taipei 11492, Taiwan*

We present a theoretical model for realizing squeezed lasing in a trapped-ion system without relying on engineered baths or tailored dissipative reservoirs. Our approach leverages the intrinsic ion-phonon interactions, where two trapped ions, each interacting with a shared vibrational mode, are driven on both red- and blue-sideband transitions. This enables the creation of a squeezed state of motion through the dynamic coupling between the ions' internal states and the phonon mode. Unlike traditional methods that require bath engineering, our model demonstrates that squeezed lasing can be achieved through a direct manipulation of ion-phonon interactions, with no external reservoirs required. We explore the steady-state behavior of the system, analyzing the onset of lasing, gain-loss balance, and the role of the squeezing parameter in shaping the phonon field's statistical properties. Furthermore, we show how external coherent drives can stabilize phase coherence and achieve controlled quadrature squeezing, offering a simple yet effective method for achieving squeezed lasing in quantum mechanical systems. Our findings provide new insights into the realization of squeezed states in phonon-based systems, with potential applications in quantum metrology and information processing.

## I. INTRODUCTION

Laser technology plays an indispensable role in various fields, from scientific research to industrial applications and consumer electronics. The distinctive features of optical lasers, including their quantum coherence and long-range propagation, have made them vital tools in modern quantum engineering and communication. In recent years, there has been a growing interest in the acoustic counterpart of lasing phenomena, specifically phonon lasing. This research extends the framework of quantum optics to explore mechanical degrees of freedom, which share fundamental mathematical similarities with photonic systems. Phonons, with their slower dynamics compared to photons, allow for more controlled manipulation of system parameters, enabling precise phase control within a given period. Furthermore, unlike photons, phonons can be coupled to atomic systems deterministically through state-dependent kicks, as seen in trapped-ion quantum computing and simulation [1], offering an advantage over the probabilistic photon-atom interaction.

Phonon lasers have emerged as a promising platform for quantum technologies, with potential applications in quantum computing [2–11], communications [12, 13], and metrology [14–20]. The first demonstration of a phonon laser in a trapped-ion system driven by optical forces [21] marked a significant milestone, showing self-sustained oscillations beyond a certain threshold in a single ion, driven by optical energy. Following this breakthrough, numerous proposals and experimental demonstrations have been conducted in a variety of platforms, such as trapped ions [22–24], quantum dots [25–27], optomechanical systems [27–36].

A variety of important laser-like properties have been observed in phonon systems, including threshold behavior [21, 28, 30, 31, 33, 35–37], Poissonian statistics [35], linewidth narrowing [28–30, 33, 35, 37], injection locking [22, 23], mode competition [31, 36], and phase control [38]. While these methods are effective in realizing lasing behavior in certain systems, they often lack flexibility, as key system parameters, such as the lasing resonator or dissipation pathways, are

fixed once designed, making in-situ reconfiguration challenging.

On the other hand, squeezed laser systems in optical setups have typically relied on bath engineering to induce squeezing, where engineered dissipative environments are used to tailor the quantum statistics of the emitted field [39, 40]. Here, we take a different route: squeezing arises from coherent ion-phonon interactions and can be absorbed into a redefinition of the motional mode, without altering the underlying gain and loss mechanisms. This separation allows squeezed lasing to be realized without bath engineering, while preserving the standard laser threshold physics.

We implement this idea in a minimal trapped-ion setting, where two ions are coupled to a shared vibrational mode and simultaneously driven on their red- and blue-sideband transitions. These coherent drives generate effective ion-phonon interactions that realize squeezed dynamics directly at the level of the motional mode, without introducing additional dissipative channels. The resulting scheme remains experimentally simple, while providing a controllable platform for exploring squeezed-lasing physics in isolated mechanical systems.

This paper is organized as follows. In Sec. II, we introduce the theoretical model and show how the driven ion-phonon interactions can be mapped onto a squeezed-mode laser description. In Sec. III, we analyze the signatures of squeezed lasing, including threshold behavior, phonon statistics, and linewidth narrowing. In Sec. IV, we study phase symmetry breaking and demonstrate how an external coherent drive enables controlled quadrature squeezing. In Sec. V, we discuss the experimental feasibility of our scheme in current trapped-ion platforms. Finally, Sec. VI summarizes our results and outlines possible extensions.

## II. THEORETICAL MODEL

We consider a physical system comprising two trapped ions coupled to a shared quantized vibrational mode of the ion crystal, representing a common axial motional degree of free-

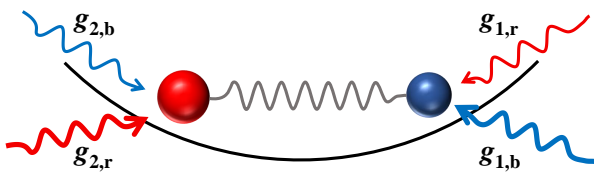


FIG. 1. Schematic of the bath-free squeezed phonon laser configuration. Two ions are driven asymmetrically on their red- and blue-sideband transitions. One ion acts as a heating agent to provide gain, while the other acts as a cooling agent to introduce loss for the shared motional mode. This setup generalizes the standard phonon laser architecture to the squeezed domain by leveraging intrinsic ion-phonon interactions without the need for external reservoir engineering.

dom. The vibrational mode is described by the bosonic annihilation and creation operators  $a$  and  $a^\dagger$ , respectively. As illustrated in the configuration in Fig. 1, the two ions are assigned distinct functional roles: one ion serves as a heating agent to provide gain, while the other facilitates cooling to introduce controlled loss.

To realize the proposed squeezed-lasing dynamics, both ions are simultaneously driven on their respective red- and blue-motional sidebands. This dual-tone driving scheme enables coherent Jaynes-Cummings (JC) and anti-Jaynes-Cummings (AJC) interactions between the ions' internal electronic states and the shared phonon mode. Under the rotating-wave approximation and within the Lamb-Dicke regime, the total interaction Hamiltonian is given by

$$H = \sum_{i=1,2} (g_{i,b} a^\dagger \sigma_i^+ + g_{i,b}^* a \sigma_i^- + g_{i,r} a \sigma_i^+ + g_{i,r}^* a^\dagger \sigma_i^-) \quad (1)$$

where  $\sigma_i^+$  and  $\sigma_i^-$  are the raising and lowering operators for the internal states of ion  $i = 1, 2$ . The coupling strengths  $g_{i,b/r} = |g_{i,b/r}| e^{-i\phi_{i,b/r}}$  describe the effective interaction strengths for blue-sideband and red-sideband transitions, respectively, with  $\phi_{i,b/r}$  the associated phases.

The physical mechanism for achieving squeezing in this model relies on the mapping of the system onto a standard laser framework within a squeezed basis. To identify the intrinsic squeezing dynamics, we define the unitary squeezing transformation

$$S(r, \theta) = \exp \left[ \frac{r}{2} \left( e^{-i\theta} a^2 - e^{i\theta} a^{\dagger 2} \right) \right], \quad (2)$$

where  $r$  is the squeezing parameter and  $\theta$  is the squeezing phase. By appropriately choosing the drive parameters such that  $\tanh(r) = \left| \frac{g_{1,r}}{g_{1,b}} \right| = \left| \frac{g_{2,b}}{g_{2,r}} \right| < 1$ , and aligning the optical phases  $\theta = \phi_{1,r} - \phi_{1,b} = \phi_{2,r} - \phi_{2,b}$ , the Hamiltonian in Eq. 1 can be reparameterized as

$$H = g_1 \cosh(r) a^\dagger \sigma_1^+ + g_1 \sinh(r) a \sigma_1^+ + g_2 \sinh(r) a^\dagger \sigma_2^+ + g_2 \cosh(r) a \sigma_2^+ + \text{h.c.}, \quad (3)$$

where  $g_1 \equiv \sqrt{|g_{1,b}|^2 - |g_{1,r}|^2}$  and  $g_2 \equiv \sqrt{|g_{2,r}|^2 - |g_{2,b}|^2}$  denote effective coupling strengths. The physical significance of this reparameterization becomes evident when applying the squeezing transformation to the mode operators. Specifically, the system is formally equivalent to a standard laser model  $H_{sq} = g_1 b^\dagger \sigma_1^+ + g_2 b \sigma_2^+ + \text{h.c.}$  acting on the squeezed mode defined by  $b = S a S^\dagger$ .

In this representation,  $H_{sq}$  takes the exact form of the dual-species Hamiltonian implemented by Ref. [24], where gain and loss are independently provided by heating (AJC) and cooling (JC) interactions, respectively. While the setup in Ref. [24] operates on the bare motional mode, our model demonstrates that by leveraging the intrinsic ion-phonon interactions via dual-tone driving, the same laser-like dynamics are engineered to act directly on a squeezed mode. This approach allows for the generation of squeezed lasing in the laboratory basis without the need for additional external reservoir engineering.

In the following sections, we numerically explore the steady-state behavior of the model across a range of parameters. We first analyze the onset of lasing and the associated nonclassical phonon statistics, including gain-loss balance, intensity correlations, and spectral narrowing. We then examine the role of the squeezing parameter in shaping the statistical properties of the phonon field. Finally, we demonstrate how an external coherent drive can break the intrinsic phase symmetry and enable controlled quadrature squeezing of the phonon mode.

### III. SIGNATURES OF SQUEEZED LASING

The transition into the squeezed-lasing regime is characterized by the emergence of a displaced squeezed coherent state from an initial squeezed vacuum. We begin our analysis by examining the system's behavior in the limit  $g_1 \rightarrow 0$ . In this regime, as reproduced in Fig. 2(a), the model reduces to an incoherent phonon-pumping scheme previously studied in the context of dark squeezed states [41]. However, as the effective heating coupling  $g_1$  increases and the system enters the lasing regime, the steady-state Wigner function undergoes a fundamental transformation. As shown in Fig. 2(b), the distribution develops a displaced, elliptically deformed structure, corresponding to a squeezed coherent state with a randomly selected phase.

To quantify the lasing transition, we first analyze the effective gain and loss mechanisms induced by the driven ions. Following the adiabatic elimination of the internal dynamics (Appendix A), the gain and decay operators are given by

$$\mathcal{G} = -\frac{|g_1|^2}{\gamma_1} \sigma_{1,z}, \quad \mathcal{K} = -\frac{|g_2|^2}{\gamma_2} \sigma_{2,z}, \quad (4)$$

where  $\gamma_1$  and  $\gamma_2$  are the spontaneous decay rates of the two ions. A crucial physical insight of our model is that these operators depend solely on the effective coupling strengths and internal decay rates, remaining entirely independent of the squeezing parameter  $r$ . This independence confirms that

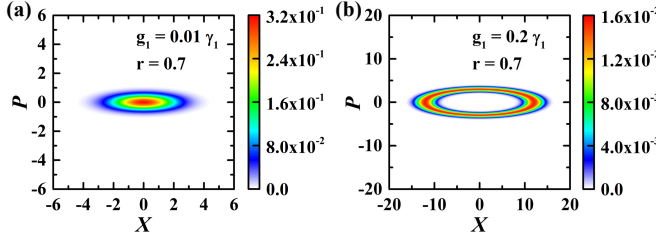


FIG. 2. Steady-state Wigner functions of the phonon mode. (a) Below-threshold regime at  $g_1 = 0.01 \gamma_1$ , exhibiting a near-symmetric profile characteristic of a squeezed vacuum state. (b) Above-threshold regime at  $g_1 = 0.2 \gamma_1$ , showing a displaced, elliptically deformed structure consistent with a random-phase squeezed coherent state. Simulation parameters are fixed at  $g_2 = 0.15 \gamma_1$  and  $\gamma_2 = 2.5 \gamma_1$ .

while squeezing reshapes the mode structure, it does not directly alter the net gain-loss balance.

In Fig. 3(a), we plot the steady-state ratio  $\langle \mathcal{G} \rangle / \langle \mathcal{K} \rangle$  as a function of the effective heating coupling  $g_1$ . A distinct threshold behavior is observed near the critical point  $g_{1,\text{th}} \approx 0.12 \gamma_1$ , above which the gain overcomes the losses and the system transitions into the lasing regime.

The establishment of coherence is further evidenced by the steady-state second-order correlation function  $g^{(2)}(0) \equiv \langle a^\dagger(0)a^\dagger(\tau)a(\tau)a(0) \rangle / \langle a^\dagger(\tau)a(\tau) \rangle^2|_{\tau=0}$  and the mean phonon number  $\langle n \rangle = \langle a^\dagger a \rangle$ , shown in Fig. 3(b). As  $g_1$  surpasses the threshold,  $g^{(2)}(0)$  decreases while  $\langle n \rangle$  rises, indicating the emergence of coherence from a nonclassical vacuum state. This transition is accompanied by linewidth narrowing in the emission spectrum, which follows a Lorentzian profile:

$$S(\omega) = \frac{n_{\text{ss}}}{\omega^2 + \Gamma^2/4} \quad (5)$$

where  $n_{\text{ss}}$  is the steady-state phonon number and  $\Gamma = \langle \mathcal{K} \rangle - \langle \mathcal{G} \rangle$  represents the effective emission linewidth. Figures 3(c) and (d) clearly illustrate linewidth narrowing above the lasing threshold, confirming the buildup of phase coherence as the gain approaches the loss rate.

A key advantage of our "bath-free" scheme is that the squeezing parameter  $r$  can be continuously tuned via the ratio of red and blue sideband couplings. To investigate its impact on lasing statistics, we fix the system well above threshold and explore the dependence of  $\langle n \rangle$  and  $g^{(2)}(0)$  on  $r$  in Fig. 4. The analytical expressions for these statistical properties are given by

$$\langle n \rangle = |\alpha_s|^2 \cosh(2r) + \sinh^2(r), \quad (6)$$

$$g^{(2)}(0) = \frac{1}{4 \langle n \rangle^2} \left[ 3 |\alpha_s|^2 \left( |\alpha_s|^2 + 2 \right) \cosh(4r) + \left( 3 \cosh(2r) - 8 |\alpha_s|^2 - 4 \right) \cosh(2r) + \left( |\alpha_s|^2 + 1 \right)^2 \right], \quad (7)$$

where  $|\alpha_s|^2$  denotes the coherent excitation amplitude in the squeezed frame. As shown in Fig. 4, our numerical results

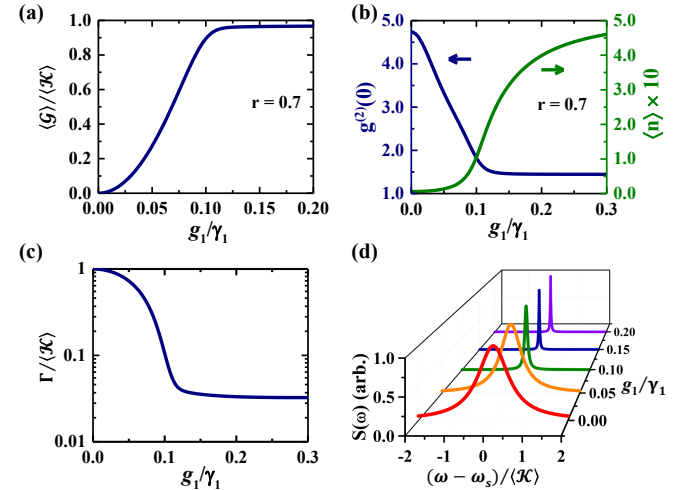


FIG. 3. Signatures of the squeezed-lasing transition. (a) Steady-state ratio of gain to loss,  $\langle \mathcal{G} \rangle / \langle \mathcal{K} \rangle$ , as a function of the effective heating coupling  $g_1$ , with the threshold identified at  $g_{1,\text{th}} \approx 0.12 \gamma_1$ . (b) Second-order coherence  $g^{(2)}(0)$  (left axis) and mean phonon number  $\langle n \rangle$  (right axis) of the phonon mode as functions of  $g_1$ . (c) Emission linewidth  $\Gamma$  versus  $g_1$ , demonstrating linewidth narrowing above the threshold. (d) Normalized emission spectrum  $S(\omega)$  for various  $g_1 / \gamma_1$ , where frequency is defined relative to the squeezed mode frequency  $\omega_s$ .

show excellent agreement with these analytical predictions. In the strongly squeezed regime ( $r \gg 1$ ),  $g^{(2)}(0)$  saturates to approximately 1.5, reflecting an intermediate phonon bunching behavior that exceeds the fluctuations of a standard coherent state but remains below those of a thermal state.

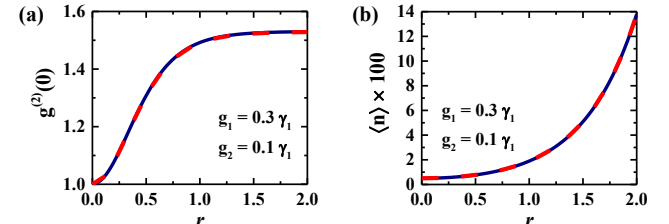


FIG. 4. Dependence of phonon statistics on the squeezing parameter  $r$  in the above-threshold regime. (a) Second-order coherence function  $g^{(2)}(0)$  and (b) mean phonon number  $\langle n \rangle$  as functions of  $r$ . Solid curves represent numerical results from the master equation, while dashed curves indicate analytical predictions based on the mapping to the squeezed frame. All results are obtained well above the lasing threshold.

#### IV. PHASE SYMMETRY BREAKING AND QUADRATURE SQUEEZING

While the squeezed-lasing regime inherently exhibits a randomly distributed phase, the phase coherence of the emitted phonon field can be stabilized by applying an external

drive with a well-defined reference. Experimentally, this is implemented by applying two resonant oscillating forces directly to the phonon mode via an electrode of the ion trap. The resulting driving Hamiltonian takes the form  $H_{d,s} = g_{d,1} (ae^{i\phi_1} + a^\dagger e^{-i\phi_1}) + g_{d,2} (ae^{i\phi_2} + a^\dagger e^{-i\phi_2})$ , where  $g_{d,1}, g_{d,2}$  and  $\phi_1, \phi_2$  denote the amplitudes and phases of the two coherent drives, respectively. By appropriately choosing the amplitude ratio and relative phase of the driving forces, the external drive can be engineered to match the same squeezing parameters  $r$  and  $\theta$  that define the internal squeezed-lasing dynamics. Specifically, we identify the matching conditions as  $\tanh(r) = \left| \frac{g_{d,2}}{g_{d,1}} \right| < 1$ , and  $\theta = -\phi_1 - \phi_2$ .

To avoid overwhelming the intrinsic lasing behavior and to ensure compatibility with the squeezed-lasing steady state, we choose weak driving amplitudes, such as  $g_{d,1} = 0.015\gamma_1$  and  $g_{d,2} = 0.009\gamma_1$ , corresponding to a moderate squeezing amplitude  $r = 0.7$ .

The influence of the external drive is clearly visible in the steady-state Wigner function shown in Fig. 5(a). The application of these weak phase-stabilizing forces results in a displacement of the phonon field in phase space and breaks the continuous phase symmetry, leading to a well-defined phase orientation for the squeezed state.

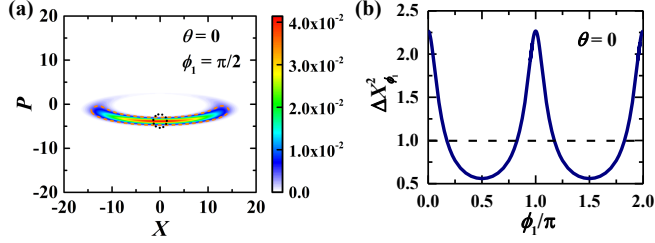


FIG. 5. Phase-symmetry breaking and quadrature squeezing. (a) Steady-state Wigner function in the presence of a weak phase-stabilizing field. Dashed orange lines indicate the 0.1 contour of the Wigner distribution, compared to the black dotted contours of a coherent state with equal amplitude. (b) Quadrature variance  $\Delta X_{\phi_1}^2$  as a function of the drive phase  $\phi_1$ , with the dashed line marking the vacuum-level fluctuations. Quadrature squeezing ( $\Delta X_{\phi_1}^2 < 1$ ) is observed near  $\phi_1 = 0.5\pi$  and  $1.5\pi$ . Shared parameters:  $g_1 = 0.2\gamma_1, g_2 = 0.15\gamma_1, \gamma_2 = 2.5\gamma_1, \theta = 0$ ; panel (a) uses  $\phi_1 = \pi/2$ .

To probe phase-sensitive properties, we vary the drive phase  $\phi_1$  while keeping the system well above the lasing threshold. The corresponding quadrature fluctuations, measured along different phase axes, exhibit a strong dependence on  $\phi_1$ . We define the generalized quadrature operator as  $X_{\phi_1} \equiv ae^{-i\phi_1} + a^\dagger e^{i\phi_1}$ , where the standard quadratures correspond to  $X = X_0$  and  $P = X_{\pi/2}$ . For reference, the vacuum fluctuation level is normalized to  $\Delta X_{\phi_1}^2 = 1$ .

As shown in Fig. 5(b), the quadrature variance drops below the vacuum level for specific phase values near  $\phi_{d,1} = 0.5\pi$ , and  $1.5\pi$ , indicating the presence of genuine quadrature squeezing. This demonstrates that the external drive not only stabilizes the phase but also enables precise control over the squeezing axis. Such control allows noise suppression to be

optimized along targeted quadrature directions, a feature particularly valuable for practical applications in quantum sensing.

## V. EXPERIMENTAL IMPLEMENTATION IN A TRAPPED-ION SYSTEM

Our theoretical model assumes two effective two-level systems coupled to a shared vibrational mode and driven on both red- and blue-sideband transitions [see Eq. 1]. We now outline how this situation can be engineered in existing trapped-ion platforms, and in particular how it can be naturally implemented by modifying the two-species phonon-laser setup of Behr *et al.* [24].

In that experiment, a mixed chain of  $^{40}\text{Ca}^+$  and  $^9\text{Be}^+$  ions is confined in a linear Paul trap and coupled to a common axial motional mode with frequency  $\omega_m$  in the megahertz range. The calcium ion realizes a JC interaction on the red sideband of an optical qubit transition, while the beryllium ion realizes an AJC interaction on the blue sideband of a hyperfine qubit. Optical pumping via short-lived excited states provides controlled dissipation for each ion, leading to competing cooling and heating channels for the shared phonon mode and giving rise to a phonon-lasing transition at low mean phonon numbers  $\bar{n} \lesssim 10$ .

To realize the squeezed-lasing Hamiltonian in Eq. 3, each ion must experience both red- and blue-sideband couplings with independently tunable amplitudes  $g_{i,r}$  and  $g_{i,b}$ . This can be implemented by adding an extra sideband tone to each ion in the above configuration. For the “cooling” ion, one supplements the red-sideband laser with a weaker blue-sideband tone at the same trap frequency, realizing effective couplings  $(g_{2,r}, g_{2,b})$ . Likewise, for the “heating” ion one adds a red-sideband tone in addition to the existing blue-sideband drive, realizing  $(g_{1,r}, g_{1,b})$ . By adjusting the relative intensities and optical phases, the squeezing parameter and phase,  $\tanh(r) = \left| \frac{g_{1,r}}{g_{1,b}} \right| = \left| \frac{g_{2,b}}{g_{2,r}} \right| < 1$ , and  $\theta = \phi_{1,r} - \phi_{1,b} = \phi_{2,r} - \phi_{2,b}$  can be tuned to the desired values.

The dissipative ingredients required for our gain and loss operators  $\mathcal{G}$  and  $\mathcal{K}$  in Eq. 4 are already present: optical pumping on the calcium and beryllium ions sets the decay rates  $\gamma_2$  and  $\gamma_1$ , respectively. In the regime  $\gamma_{1,2} \gg g_{1,2}$ , which is satisfied for sideband Rabi frequencies of a few kilohertz and optical pumping rates in the tens to hundreds of kilohertz, the internal dynamics can be adiabatically eliminated and the phonon mode obeys the simple gain-loss master equation used in our analysis. Typical trap parameters (axial frequencies in the megahertz range and Lamb-Dicke parameters of order  $10^{-2} - 10^{-1}$ ) permit tuning of the sideband couplings over at least an order of magnitude via the laser intensities. This allows one to access both the below-threshold regime, where the phonon mode is close to a squeezed-vacuum-like state, and the above-threshold regime, where our theory predicts a displaced squeezed steady state with partial phonon bunching and linewidth narrowing.

Phase locking of the lasing mode can be realized by applying a weak resonant oscillating force to a trap electrode,

providing the coherent drive used in Sec. IV. Matching the drive phase to the intrinsic squeezing parameters  $r$  and  $\theta$  implements the symmetry-breaking mechanism that stabilizes a particular quadrature of motion and allows direct measurements of quadrature squeezing. Importantly, all of these steps involve only coherent sideband drives and standard optical pumping—no squeezed reservoirs, parametric cavity drives, or other forms of reservoir engineering are required to realize squeezed phonon lasing in this setup.

## VI. DISCUSSION AND CONCLUSION

Our results demonstrate that squeezed-lasing behavior can be achieved in a minimal trapped-ion system consisting of two ions coupled to a shared vibrational mode, without the need for engineered dissipation or external reservoirs. This approach contrasts with previous schemes for squeezed lasers in optical and superconducting systems, which typically rely on engineered baths to shape the steady-state quantum statistics of the emitted field. In our approach, squeezed lasing emerges purely from coherent ion-phonon interactions, achieved by simultaneously driving the ions on their red- and blue-sideband transitions. These interactions induce effective squeezed couplings between the ions and the phonon mode, generating the desired squeezed state through intrinsic control mechanisms.

By analyzing the steady-state behavior of the system under varying coupling strengths, we identify a clear lasing threshold characterized by the balance of gain and loss, the buildup of coherent excitation, and spectral narrowing. Above threshold, the system supports a squeezed coherent phonon state with tunable statistical properties. The squeezing parameter  $r$  can be adjusted by varying the ratio of red- and blue-sideband couplings, providing direct control over both the mean phonon number and the second-order correlation function. In the strongly squeezed regime, we observe partial phonon bunching, which is indicative of a nonclassical, non-Poissonian steady state.

Furthermore, we have shown that the intrinsic phase symmetry of the system can be explicitly broken by applying a weak external drive. This drive not only selects a well-defined phase for the lasing mode but also facilitates the observation of quadrature squeezing below the vacuum level. This feature is particularly valuable for practical applications, as it enables noise suppression in targeted quadratures while maintaining overall coherence.

Taken together, these findings establish a new direction for realizing nonclassical light-like states in trapped-ion systems. By eliminating the need for bath engineering, our work simplifies both the theoretical modeling and experimental implementation, offering a cleaner and more controllable approach to exploring squeezed-lasing physics. Our approach opens new possibilities for integrating squeezed phonon states into quantum sensing and information protocols, and extends the concept of squeezed lasing to other isolated bosonic systems beyond optics.

## ACKNOWLEDGMENTS

We acknowledge support from the National Science and Technology Council (NSTC), Taiwan, under Grant No. NSTC-113-2112-M-002-025 and No. NSTC-112-2112-M-002-001. We are also grateful for support from TG 1.2 of NCTS at NTU.

## APPENDIX A: Derivation of Gain, Decay, and Linewidth

In this appendix, we derive the gain, decay, and linewidth expressions used to characterize the spectral properties of the squeezed-lasing system.

### 1. Gain and Decay Operators

We begin by examining the equations of motion for the system operators in the Heisenberg picture, derived from the Hamiltonian in Eq. 3. The evolution of the phonon annihilation operator  $a$  and the internal atomic operators is given by:

$$\begin{aligned} \partial_t a &= -ig_1 \cosh(r) \sigma_1^+ - ig_1^* \sinh(r) \sigma_1^- \\ &\quad - ig_2 \sinh(r) \sigma_2^+ - ig_2^* \cosh(r) \sigma_2^-, \\ \partial_t \sigma_1^- &= -\frac{\gamma_1}{2} \sigma_1^- + ig_1 \cosh(r) a^\dagger \sigma_{1,z} + ig_1 \sinh(r) \sigma_{1,z} a, \\ \partial_t \sigma_2^- &= -\frac{\gamma_2}{2} \sigma_2^- + ig_2 \sinh(r) a^\dagger \sigma_{2,z} + ig_2 \cosh(r) \sigma_{2,z} a, \\ \partial_t \sigma_{1,z} &= -\gamma_1 (\sigma_{1,z} + 1) - 2ig_1 \cosh(r) a^\dagger \sigma_1^+ + 2ig_1^* \cosh(r) a \sigma_1^- \\ &\quad - 2ig_1 \sinh(r) a \sigma_1^+ + 2ig_1^* \sinh(r) a^\dagger \sigma_1^-, \\ \partial_t \sigma_{2,z} &= -\gamma_2 (\sigma_{2,z} + 1) - 2ig_2 \sinh(r) a^\dagger \sigma_2^+ + 2ig_2^* \sinh(r) a \sigma_2^- \\ &\quad - 2ig_2 \cosh(r) a \sigma_2^+ + 2ig_2^* \cosh(r) a^\dagger \sigma_2^-. \end{aligned}$$

We consider the regime  $\gamma_{1,2} \gg g_{1,2}$ , where the internal dynamics of the ions reach a steady state on a time scale much shorter than the evolution of the phonon mode. Therefore, we can assume the steady state for the spin variables ( $\partial_t \sigma_{1/2}^- = 0$  and  $\partial_t \sigma_{1/2,z} = 0$ ) and obtain the following evolution equation for the phonon mode:

$$\begin{aligned} \partial_t a &= -\frac{|g_1|^2}{\frac{\gamma_1}{2}} \sigma_{1,z} a + \frac{|g_2|^2}{\frac{\gamma_2}{2}} \sigma_{2,z} a \\ &\equiv \frac{1}{2} \mathcal{G} a - \frac{1}{2} \mathcal{K} a, \end{aligned}$$

where  $\mathcal{G}$  and  $\mathcal{K}$  are the gain and decay operators, respectively. They are defined as

$$\begin{aligned} \mathcal{G} &= -\frac{|g_1|^2}{\gamma_1} \sigma_{1,z}, \\ \mathcal{K} &= -\frac{|g_2|^2}{\gamma_2} \sigma_{2,z}. \end{aligned}$$

These operators represent the effective gain and decay rates due to the interaction of the ions with the phonon mode.

## 2. Laser Linewidth

To calculate the laser linewidth, we can perform the Fourier transformation of the two-time correlation function  $\langle a^\dagger(\tau)a(0) \rangle$ . Since the system is in the steady state, the expectation values of both gain and decay operators are constant, and the equation for  $a(t)$  is given by:

$$\dot{a}(t) = \frac{1}{2} (\langle \mathcal{G} \rangle - \langle \mathcal{K} \rangle) a(t).$$

The corresponding correlation function is:

$$\begin{aligned} \langle a^\dagger(\tau)a(0) \rangle &= \langle a^\dagger(0)a(0) \rangle e^{\frac{1}{2}(\langle \mathcal{G} \rangle - \langle \mathcal{K} \rangle)\tau} \\ &\equiv \langle a^\dagger(0)a(0) \rangle e^{-\frac{\Gamma}{2}\tau}, \end{aligned}$$

where the linewidth is  $\Gamma = (\langle \mathcal{K} \rangle - \langle \mathcal{G} \rangle)$ . The spectral line-shape of the system is then given by:

$$S(\omega) = \langle a^\dagger(0)a(0) \rangle \mathcal{F}\left(e^{-\frac{\Gamma}{2}\tau}\right) = \frac{n_{ss}}{\omega^2 + \frac{\Gamma^2}{4}},$$

where  $n_{ss}$  is the steady-state phonon number and  $\mathcal{F}$  is the Fourier transform operation.

---

[1] J. I. Cirac and P. Zoller, *Phys. Rev. Lett.* **74**, 4091 (1995).

[2] K.-A. B. Soderberg and C. Monroe, *Rep. Prog. Phys.* **73**, 036401 (2010).

[3] R. Ruskov and C. Tahan, *J. Phys: Conf. Ser.* **398**, 012011 (2012).

[4] C. M. Reinke and I. El-Kady, *AIP Adv.* **6**, 122002 (2016).

[5] C. Flühmann, T. L. Nguyen, M. Marinelli, V. Negnevitsky, K. Mehta, and J. P. Home, *Nature* **566**, 513 (2019).

[6] W. Ge, B. C. Sawyer, J. W. Britton, K. Jacobs, J. J. Bollinger, and M. Foss-Feig, *Phys. Rev. Lett.* **122**, 030501 (2019).

[7] J. Loyer, J. Lages, and D. L. Shepelyansky, *Phys. Rev. A* **101**, 032349 (2020).

[8] H. Gan, G. Maslennikov, K.-W. Tseng, C. Nguyen, and D. Matsukevich, *Physical Review Letters* **124**, 170502 (2020).

[9] C.-H. Nguyen, K.-W. Tseng, G. Maslennikov, H. C. J. Gan, and D. Matsukevich, arXiv 10.48550/ARXIV.2104.04168 (2021), arXiv:2104.04168 [quant-ph].

[10] W. Chen, J. Gan, J.-N. Zhang, D. Matsukevich, and K. Kim, *Chin. Phys. B* **30**, 060311 (2021).

[11] K. Wan, S. Choi, I. H. Kim, N. Shutty, and P. Hayden, *PRX Quantum* **2**, 040345 (2021).

[12] A. Bienfait, K. J. Satzinger, Y. P. Zhong, H.-S. Chang, M.-H. Chou, C. R. Conner, É. Dumur, J. Grebel, G. A. Peairs, R. G. Povey, and A. N. Cleland, *Science* **364**, 368 (2019).

[13] É. Dumur, K. J. Satzinger, G. A. Peairs, M.-H. Chou, A. Bienfait, H.-S. Chang, C. R. Conner, J. Grebel, R. G. Povey, Y. P. Zhong, and A. N. Cleland, *npj Quantum Inf.* **7**, 173 (2021).

[14] D. A. R. Dalvit, R. L. de Matos Filho, and F. Toscano, *New J. Phys.* **8**, 276 (2006).

[15] C. Sabín, D. E. Bruschi, M. Ahmadi, and I. Fuentes, *New J. Phys.* **16**, 085003 (2014).

[16] D. Hu, L. Niu, S. Jin, X. Chen, G. Dong, J. Schmiedmayer, and X. Zhou, *Commun. Phys.* **1**, 29 (2018).

[17] F. Wolf, C. Shi, J. C. Heip, M. Gessner, L. Pezzè, A. Smerzi, M. Schulte, K. Hammerer, and P. O. Schmidt, *Nat. Commun.* **10**, 2929 (2019).

[18] M. Drechsler, M. B. Farías, N. Freitas, C. T. Schmiegelow, and J. P. Paz, *Phys. Rev. A* **101**, 052331 (2020).

[19] J. Cerrillo and D. Rodríguez, *Europhys. Lett.* **134**, 38001 (2021).

[20] A. Delakouras, D. Rodríguez, and J. Cerrillo, arXiv 10.48550/ARXIV.2202.00626 (2022), arXiv:2202.00626 [quant-ph].

[21] K. Vahala, M. Herrmann, S. Knünz, V. Batteiger, G. Saathoff, T. W. Hänsch, and T. Udem, *Nat. Phys.* **5**, 682 (2009).

[22] S. Knünz, M. Herrmann, V. Batteiger, G. Saathoff, T. W. Hänsch, K. Vahala, and T. Udem, *Phys. Rev. Lett.* **105**, 013004 (2010).

[23] M. Ip, A. Ransford, A. M. Jayich, X. Long, C. Roman, and W. C. Campbell, *Phys. Rev. Lett.* **121**, 043201 (2018).

[24] T. Behrle, T. Nguyen, F. Reiter, D. Baur, B. de Neeve, M. Stadler, M. Marinelli, F. Lancellotti, S. Yelin, and J. Home, *Physical Review Letters* **131**, 043605 (2023).

[25] J. Kabuss, A. Carmele, T. Brandes, and A. Knorr, *Phys. Rev. Lett.* **109**, 054301 (2012).

[26] J. Kabuss, A. Carmele, and A. Knorr, *Phys. Rev. B* **88**, 064305 (2013).

[27] A. Khaetskii, V. N. Golovach, X. Hu, and I. Žutić, *Phys. Rev. Lett.* **111**, 186601 (2013).

[28] I. S. Grudinin, H. Lee, O. Painter, and K. J. Vahala, *Phys. Rev. Lett.* **104**, 083901 (2010).

[29] R. P. Beardsley, A. V. Akimov, M. Henini, and A. J. Kent, *Phys. Rev. Lett.* **104**, 085501 (2010).

[30] I. Mahboob, K. Nishiguchi, A. Fujiwara, and H. Yamaguchi, *Phys. Rev. Lett.* **110**, 127202 (2013).

[31] U. Kemiktarak, M. Durand, M. Metcalfe, and J. Lawall, *Phys. Rev. Lett.* **113**, 030802 (2014).

[32] H. Jing, S. K. Özdemir, X.-Y. Lü, J. Zhang, L. Yang, and F. Nori, *Phys. Rev. Lett.* **113**, 053604 (2014).

[33] J. Zhang, B. Peng, Ş. K. Özdemir, K. Pichler, D. O. Krimer, G. Zhao, F. Nori, Y.-x. Liu, S. Rotter, and L. Yang, *Nat. Photonics* **12**, 479 (2018).

[34] Y. Jiang, S. Maayani, T. Carmon, F. Nori, and H. Jing, *Phys. Rev. Applied* **10**, 064037 (2018).

[35] R. M. Pettit, W. Ge, P. Kumar, D. R. Luntz-Martin, J. T. Schultz, L. P. Neukirch, M. Bhattacharya, and A. N. Vamivakas, *Nat. Photonics* **13**, 402 (2019).

[36] J. Sheng, X. Wei, C. Yang, and H. Wu, *Phys. Rev. Lett.* **124**, 053604 (2020).

[37] J. B. Khurgin, M. W. Pruessner, T. H. Stievater, and W. S. Rabinovich, *Phys. Rev. Lett.* **108**, 223904 (2012).

[38] Y.-L. Zhang, C.-L. Zou, C.-S. Yang, H. Jing, C.-H. Dong, G.-C. Guo, and X.-B. Zou, *New J. Phys.* **20**, 093005 (2018).

[39] C. Navarrete-Benlloch, J. J. García-Ripoll, and D. Porras, *Physical Review Letters* **113**, 193601 (2014).

[40] C. Sánchez Muñoz and D. Jaksch, *Physical Review Letters* **127**, 183603 (2021).

[41] J. I. Cirac, A. S. Parkins, R. Blatt, and P. Zoller, *Physical Review Letters* **70**, 556 (1993).